Gold Colloid-Nanostructured Surfaces for Enhanced Piezoelectric Immunosensing of Staphylococcal Enterotoxin A

Maroua Ben Haddada, Michèle Salmain, Souhir Boujday

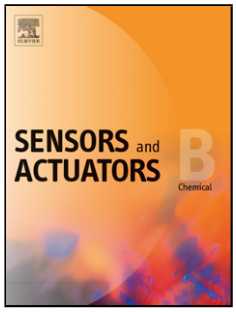

Title: Gold Colloid-Nanostructured Surfaces for Enhanced Piezoelectric Immunosensing of Staphylococcal Enterotoxin A

Authors: Maroua Ben Haddada, Michèle Salmain, Souhir Boujday

PII: S0925-4005(17)31612-X
DOI: http://dx.doi.org/10.1016/j.snb.2017.08.180
Reference: SNB 23047

To appear in: *Sensors and Actuators B*

Received date: 5-5-2017
Revised date: 26-7-2017
Accepted date: 23-8-2017

Please cite this article as: Maroua Ben Haddada , Michèle Salmain, Souhir Boujday, Gold Colloid-Nanostructured Surfaces for Enhanced Piezoelectric Immunosensing of Staphylococcal Enterotoxin A, Sensors and Actuators B: Chemicalhttp://dx.doi.org/10.1016/j.snb.2017.08.180

Gold Colloid-Nanostructured Surfaces for Enhanced Piezoelectric Immunosensing of Staphylococcal Enterotoxin A

Maroua Ben Haddada [1,2], Michèle Salmain [1,*], and Souhir Boujday [2,*]

[1] Sorbonne Universités, UPMC Univ Paris 06, CNRS, Institut Parisien de Chimie Moléculaire (IPCM), 4 place Jussieu, F-75005 Paris, France
[2] Sorbonne Universités, UPMC Univ Paris 06, CNRS, Laboratoire de Réactivité de Surface (LRS), UMR 7197, 4 Place Jussieu, F-75005 Paris, France

* Corresponding authors:

Tel: +33144276001, Fax: +33144276033, souhir.boujday@upmc.fr
Tel: +33144276732; Michele.salmain@upmc.fr

Highlights

- Gold- and silicon-coated quartz sensors were nanostructured with gold nanoparticles
- A capture layer comprising an anti-SEA antibody was built up on the sensor surface
- Nanostructuration improved sensor response owing to better accessibility of antibodies
- With a sandwich-type assay, the limit of detection was 1 ng SEA/mL in 25 min

Abstract

We describe the use of gold nanoparticles (AuNP) as a nanostructuring agent on quartz crystal sensor chips to engineer staphylococcal enterotoxin A (SEA) piezoelectric biosensors with amplified response. AuNPs were assembled on gold- or silicon-coated quartz crystal sensor chips by a wet chemistry process involving their chemisorption to preformed thiol and amine terminated Self-Assembled Monolayers (SAMs). The purpose of this nanostructuration was to modify the topography of the surface and improve the accessibility of the binding sites on the surface of the sensor chips. Biointerfaces, comprising a polyclonal antibody against staphylococcal enterotoxin A (SEA), were further built up on these gold nanoparticle-coated sensors and their ability to capture SEA was monitored in real time with a quartz crystal microbalance with dissipation monitoring. It was found out that, although the surface density in capture antibody was similar on both nanostructured and planar sensors, the sensor response, expressed as frequency shift recorded during the binding of SEA to the antibody, was significantly higher for the nanostructured sensors as compared to the planar ones. All the same, the limit of detection was lower for the nanostructured sensors: 8 ng/mL *vs* 20 ng/mL for the planar sensors. This was rationalized by a possibly better accessibility of the antigen binding sites rather than a consequence of specific surface increase. Using a sandwich type assay, gold nanoparticles coated silicon quartz sensor chips provided the lowest limit of detection of ca. 1 ng/mL in a total assay time of 25 min.

Keywords

Quartz crystal microbalance (QCM); biosensor; antibody; gold nanoparticles; staphylococcal enterotoxin A (SEA); protein A

1. Introduction

Foodborne poisoning owing to the consumption of food contaminated with pathogens and/or toxins is a major concern worldwide. *Staphylococcus aureus* is one of the most prevalent microorganisms involved in these diseases. Under favorable conditions, some *S. aureus* strains produce enterotoxins (SEs) whose ingestion of as low as 100 ng is sufficient to cause intoxication symptoms. Staphylococcal enterotoxin A (SEA), one of the 21 *S. aureus* toxins identified to date, is the most commonly encountered biotoxin involved in staphylococcal food poisoning outbreaks [1]. SEA is a small monomeric protein (MW = 28 kDa) with high thermal and proteolytic stability [2] so that even consumption of cooked food can be deleterious to health if contaminated.

Early detection of contaminants such as SEA is thus required to limit the spreading of cases by rapidly withdrawing suspected foodstuff from the market. Traditional microbiological methods are not able to solve this issue. Conversely, molecular methods including biosensing devices are potentially able to meet this demand since they can provide a qualitative or even a quantitative answer in a short period of time while operating on complex food samples [3, 4]. Within the last ten years, an impressive amount of literature reports dealt with the setup of immunosensors for the detection of SEs. Various immunosensing setups operating with optical [5-16], acoustic [17-21] or electrical [22, 23] transduction modes have been designed to detect SEs and showed variable working range and sensitivity. The pg/mL detection level was recently reached using a microchannel device made of microscale pillars and fluorescence detection [24, 25].
In this context, piezoelectric biosensors using quartz chips are particularly attractive since they provide quantitative information on biomolecular interactions at the solid – liquid interface in real time and label-free fashion and allow the detection of high molecular weight targets at the ng level [26]. Recently, interest has been drawn towards the contribution of nanomaterials in the development of biosensors for toxin analysis [27, 28]. Among nanomaterials, gold nanoparticles (AuNP) have attracted special interest in the field of biosensor development owing to their outstanding physico-chemical features and their ease of synthesis and functionalization [29-31]. Their assembly on planar substrates was shown to increase the response of mid-IR optical immunosensors [32, 33]. Regarding piezoelectric sensors, inclusion of gold nanoparticles has been shown to increase their sensitivity owing to surface [34-42] or mass [31, 43-48] enhancement effects. Using gold nanoparticles-nanostructured surfaces, we successfully built up a piezoelectric immunosensor for the anti-inflammatory drug diclofenac with a sensitivity up to 6 times that reached with planar substrates [49]. Furthermore, thanks to the biocompatibility of AuNPs, biomolecules immobilized on such platforms are less prone to lose their bioactivity.
In the present study, gold- and silicon-coated quartz crystal sensors were modified with gold nanoparticles according to optimized procedures [50, 51] so as to slightly increase their surface area and provide a three-dimensional topography allowing a better accessibility of the recognition sites. These nanostructured sensors were employed as platforms to design immunosensors for the piezoelectric detection of SEA (Scheme 1). This sensor configuration was compared to planar Au and Si quartz sensors in terms of working range and sensitivity.

2. Materials and methods

2.1.Reagents

Sodium citrate, gold(III) chloride trihydrate, tannic acid, Cysteamine (CEA), 1,4-phenylenediisothiocyanate (PDITC), 11-mercaptoundecanoic acid (MUA) Staphylococcal enterotoxin A (SEA), (3-aminopropyl)triethoxysilane (APTES), Bovine Serum Albumin (BSA), N-ethyl-N'-(3-(dimethylamino)propyl)carbodiimide hydrochloride (EDC), N-hydroxysuccinimide (NHS) were bought from Sigma-Aldrich. Recombinant protein A was purchased from Thermo scientific. Affinity-purified rabbit anti-SEA antibody was purchased from Toxin technology. A stock solution of SEA was prepared in water and its actual concentration determined by OD_{280nm} measurement taking ε_{280} = 38,000 $M^{-1}.cm^{-1}$. Phosphate buffered saline (PBS) and PBS containing 0.1% BSA (w/v) (PBS-BSA) were used as running buffers. Citrate-coated gold nanoparticles were synthesized according to the previously optimized procedure [52]. Briefly, to prepare 100 mL of a 13.5 nm diameter colloid solution ($AuNP_{13}$), two stock solutions were prepared: solution A: 1 mL 1% (w/v) $HAuCl_4$ and 79 mL water; solution B: 4 mL 1% sodium citrate, 0.025 mL 1% tannic acid and 16 mL water. Solutions A and B were heated to 60°C under stirring then mixed. When the solution turned red, the mixture was heated up to 95°C for few minutes and cooled on ice. 40 nm diameter colloid solutions ($AuNP_{40}$) were prepared similarly by changing the solution B accordingly: 1.34 mL 1% sodium citrate, no tannic acid and 18.66 mL water. Colloidal solutions were kept in amber glassware, stored in the refrigerator at 4°C and used within a month.

2.2.Methods

2.2.1. Assembly of AuNP on Au and Si quartz sensors

Clean Au sensor chips were dipped in a solution of cysteamine (10 mM in ethanol) for 18-24 h. In the meantime, a mixture of MUA (10 mM), EDC (60 mM) and NHS (30 mM) in ethanol was incubated for 90 min. After washing twice with ethanol, the sensors were dipped in the mixture of MUA, EDC and NHS during 90 min, then washed twice with absolute ethanol and dried under a flow of nitrogen. Clean Si sensor chips were dipped in a solution of APTES (50 mM in dry toluene) and the mixture was heated to 75°C for 24 h. In the meantime, a mixture of MUA (10 mM), EDC (60 mM) and NHS (30 mM) in ethanol was incubated for 90 min. After extensive washing with toluene, the sensor chips were exposed to the mixture of MUA, NHS and EDC for 90 min, then washed twice with absolute ethanol and dried under a flow of nitrogen.

In the immersion method, the modified sensors were dipped into freshly prepared solution of $AuNP_{13}$ (3.3 nM) or $AuNP_{40}$ (0.13 nM), with no further dilution for 90 min under gentle agitation, then washed twice in water and dried under nitrogen. In the flow method, the modified sensor chips were mounted in the QCM-D cell and a solution of $AuNP_{13}$ (0.33 nM in water) was flowed over the sensors for 45 min and then flushed with water.

2.2.2. SEA Immunosensors construction

Post-functionalization of AuNP-coated sensor chips was performed by first dipping the chips in a solution of CEA (1 mM in EtOH) during 2 h, then, in a solution of PDITC (0.02% w/v in pyridine/DMF 1:9) for 30 min and finally washing with absolute ethanol and drying under a flow of N_2. The chips were mounted in the QCM and the system was equilibrated by flowing PBS. A solution of protein A (20 mg/L in PBS) was injected for 10 min. After a washing step with PBS, anti-SEA solution (10 mg/L in PBS) was flowed for 10-12 min. After flushing with

PBS, PBS-BSA was flowed over the sensors for 10-12 min to block non specific binding sites.

2.2.3. Detection of SEA in the direct assay format

Standard solutions of SEA at 48, 97, 194, 485 and 970 ng/mL were prepared by diluting the aqueous stock solution with PBS-BSA. These solutions were injected for 10 to 12 min and flushed with PBS-BSA. The frequency shift ΔF between the beginning of injection and the end of the washing step was measured on each sensorgram.

2.2.4. **Detection of SEA in the amplified sandwich assay format**

A solution of anti-SEA (10 mg/L in PBS-BSA) was injected for 10-12 min, followed by flushing with running buffer. The cumulated frequency shift between the beginning of injection of SEA and the end of the second washing step was measured on each sensorgram.

2.2.5. **QCM-D measurements**

Piezoelectric measurements were performed with AT-cut gold- or silicon-coated quartz crystal electrodes with nominal frequency of 5 MHz (Lot-Oriel, France) in the flow-through mode (flow rate = 50 µL/min) on a quartz crystal microbalance with dissipation monitoring QCM-D (E4 model, Q-sense, Sweden) at 22°C. Before use, sensors were washed in ethanol and dried by a nitrogen gas flow. The experimental setup is described in [53]. Mass uptakes Δm were calculated with the Sauerbrey equation (1) assuming the deposited films behave as an elastic mass

(1) $\Delta F = -N \times \Delta m / C_f$

where ΔF is the frequency shift at the 5^{th} overtone, C_f (= -17.7 ng/cm^2/Hz at F = 5 MHz) the mass sensitivity factor and N (= 1,3, 5, 7 …) the overtone number.

2.2.6. Scanning electron microscopy

Scanning electron microscopy images of the gold nanoparticles on the modified Au and Si quartz crystal sensors were obtained using a FEG Hitachi SU-70 scanning electron microscope with a low voltage of 1 kV at a distance of 1.9 - 2.3 mm; the secondary electron detector "in Lens" was used. Particle densities were determined by counting the particles in the SEM images on representative area of 2.3 x 2.5 µm^2.

2.2.7. X Ray Photoelectron Spectroscopy

XPS analyses were performed using a PHOIBOS 100 X-ray photoelectron spectrometer from SPECS GmbH (Berlin, Germany) with a monochromated AlKα X-ray source (hν = 1486.6 eV) operating at P = 1×10-10 Torr or less. Spectra were carried out with a 50 eV pass energy for the survey scan and 10 eV pass energy for the elements. The spectra were fitted using Casa XPS v.2.3.15 Software (Casa Software Ltd., UK) and applying a Gaussian/Lorentzian ratio G/L equal to 70/30.

2.2.8. Polarization Modulation IR Reflection Absorption Spectroscopy

PM-IRRAS spectra were recorded on a commercial Thermo-scientific (France) Nexus spectrometer. The external beam was focused on the sample with a mirror, at an optimal incident angle of 85°. A ZnSe grid polarizer and a ZnSe photoelastic modulator, modulating the incident beam between p- and s-polarizations (HINDS Instruments, PEM 90, modulation

frequency = 37 kHz), were placed prior to the sample. The light reflected at the sample was then focused onto a nitrogen-cooled MCT detector. The presented spectra result from the sum of 128 scans recorded with 8 cm^{-1} resolution.

3. Results and discussion

3.1.Functionalization of Au and Si quartz sensors

Prior to gold nanoparticles immobilization, gold and silicon-coated quartz sensors were functionalized to introduce amine and thiol groups as drawn in Scheme 1.

On silicon substrates, whose surface is covered with a thin native silica layer, this was achieved following a previously optimized procedure [50] by first assembling aminopropyltriethoxysilane (APTES) on silanol groups, then, in a second step, by reaction between the surface amino groups and 11-mercaptoundecanoic acid (MUA) whose terminal carboxylic acid group had been converted on the side into an activated N-hydroxysuccinimide ester by reaction with NHS and EDC (Scheme 1-A). This surface chemistry leads to a Self-Assembled Monolayer (SAM) terminated by a mixture of thiols and amine with SH/NH_2 ratio (measured by X-Ray Photoelectron Spectroscopy (XPS) directly from the ratio S/N) = 0.24. This mixed SAM has been previously shown by us to afford a high density of AuNP as well as a limited number of particle aggregates [50]. We applied a similar surface chemistry to gold sensors that were sequentially treated with cysteamine to generate surface amino groups then by activated MUA (Scheme 1-B). After each step, surfaces were characterized by PM-IRRAS and XPS to determine the surface composition (Figure 1).

The spectra on Figure 1B show that the chemistry is rather complicated on gold substrates. PM-IRRAS spectra show an increase in the CH stretching vibration region (bands at 2853 and 2927 cm^{-1}) upon MUA addition evidencing its presence on the surface. In the low wavenumbers region, MUA addition also induces a modification of the spectrum; On CEA modified gold, the primary amine bands are present in the range 1660−1640 cm^{-1} and the ammonium group bands around 1530 and 1470 cm^{-1}, next to the CH_2 scissor vibration bands around 1402 cm^{-1}. Upon MUA grafting the intensity of these bands becomes lower and amide bands appear giving evidence of the successful conjugation of activated acid to surface amine groups. However, an additional band at 1734 cm^{-1} ascribable to few unreacted activated ester is present on the CEA+MUA spectra. This means either that these activated MUA molecules are simply physisorbed on the surface, or, more likely, that they substituted some CEA molecules and are directly attached to the gold surface by an Au-S bond. Since it is difficult to quantify the amount of MUA attached to surface using PM-IRRAS, we performed an XPS analysis. The chemical composition determined by XPS is summarized in table S1 (SI section). The high level of carbon shows the presence of contaminants on the substrate surfaces, very difficult to avoid considering the successive steps and the different solvents used for the assembly of CEA and the subsequent grafting of MUA. To overcome the interference of these contaminants in the analysis we focused on the relative amount of sulfur and nitrogen on the surfaces and on the N1s photopeak spectra shown in Figure 1A. The N 1s peaks included two contributions: the first at 399.8 eV is ascribable to primary amine [$C\text{-}NH_2$] and/or to amide nitrogen [$(O=C)\text{-}NH$] as it is difficult to discriminate these two nitrogen atoms [54], the second contribution at 401.6 eV is attributed to ammonium groups [$C\text{-}NH_3^+$]. The intensity of this peak is slightly lowered in the CEA-MUA modified-substrate

consequently to signal attenuation upon MUA addition. The shape of this peak is also modified upon MUA grafting, it shows a higher contribution of the amine/amide nitrogen in agreement with the successful grafting and amide band formation. In addition, the S/N ratio increases by 18% after adding activated MUA, i.e. a SAM terminated by a mixture of thiol and amine functions with a ratio thiol/amine=0.18, slightly lower than for silicon-coated sensors where thiol/amine SH/NH_2 = 0.24. Note that the value 0.18 is a maximum as some of the SH groups may be grafted on the substrates through S-Au bonds as suggested by IR spectra.

3.2.*Assembly of AuNP on Au and Si quartz sensors*

Gold nanoparticles were deposited on the functional substrates following two methods. The first is immersion, in this case the sensors were dipped in AuNPs solution and the mixture was kept under stirring for 90 min. The second method is flow, in this method the AuNPs solution is injected in a cell exposing the sensor surface using a peristaltic pump. The AuNP-functionalized sensors were subsequently analyzed by scanning electron microscopy. Figure S1 shows SEM images obtained after depositing $AuNP_{13}$ by the immersion method on silicon and gold surfaces. The images show the presence of multiple aggregates on the silicon substrates. For gold, particle dispersion on the surface appeared to be better but the analysis of other images showed that the coverage was heterogeneous with an average particle density of approx. $20x10^9$ particles/cm^2.

For the flow Method, adsorption of $AuNP_{13}$ was monitored in real time by QCM-D. The variation of frequency of the quartz at the 5^{th} overtone and the dissipation resulting from adsorption of the $AuNP_{13}$ on the gold and silicon surfaces are presented in

Figure 2 together with the SEM images obtained after particles deposition.

For the gold surface, a very small decrease of the resonance frequency was observed upon injection of $AuNP_{13}$ solution (ΔF = -1 Hz), showing a very small number of $AuNP_{13}$ adsorbing on the surface, which is in agreement with the low coverage observed on the SEM image (

Figure 2-b). For silicon, a large negative shift of the frequency, equal to 26 Hz, along with a very small variation of dissipation were observed upon injection of the gold colloid solution. This shows an important adsorption of $AuNP_{13}$ on the surface. In addition, the little change in dissipation allows the application of the Sauerbrey equation that gave a surface coverage of $18.5x10^9$ particles/cm^2. The corresponding SEM images (

Figure 2-d) corroborate the presence of a high coverage of AuNP on the surface. Counting of the number of AuNP per area unit on several SEM images (7 to 11) gave a mean density of 17.5 (±1) $x10^9$ particles/cm^2 in excellent agreement with the QCM value given above.

Regardless the method of AuNP deposition, silicon-modified surfaces adsorb a higher amount of particles than gold ones. We previously observed this behavior and attributed it to the difference of chemical groups on the two substrates: silane addition to silica chemistry offers multiple anchoring points including silanolate in addition to the amine and thiol groups, while for gold only the latter are present [49].

To conclude this part, the deposition of AuNPs under flow prevents their aggregation on silicon substrates but gives a low coverage for gold substrates. This probably results from the difference in surface terminal groups as discussed in the previous paragraph. Thus, for immunosensor construction we chose to use surfaces with similar AuNP coverages but obtained following different deposition methods: by immersion for gold substrates and under flow for silicon ones.

Let us note here that we had reached a much higher coverage (~120 x10^9 particles/cm^2) and dispersion of AuNPs by another route involving the preliminary formation of a PEG film. This strategy was used to design an immunosensor for the competitive detection of diclofenac, a small pharmaceutical pollutant [49]. Unfortunately, we could not use this strategy in the present case as all the attempts to graft proteins to these nanostructured substrates following the procedure described below were unsuccessful, most probably because of the well-known protein repulsive property of PEG films.

3.3.SEA immunosensors construction and test

We previously compared different strategies for the construction of SEA immunosensors on planar gold surfaces [55]. The most efficient sensing layer in terms of sensor response to analyte was obtained by sequential treatment of gold surfaces with cysteamine and 1,4-phenylenediisothiocyanate (PDITC) to generate amine-reactive functions for protein A immobilization (Scheme 1-C), then after covalent attachment of Protein A, the polyclonal rabbit anti-SEA antibody was immobilized on Protein A by affinity. Finally, a blocking step was achieved by adsorbing BSA prior to SEA detection. We applied the same chemistry to nanostructured sensors. To check whether covalent attachment of protein A to the surface is mandatory at this step, we attempted to simply physisorb protein A on the nanostructured layers then adsorb anti-SEA by affinity. Our QCM results clearly showed that the amount of both proteins was very low when post-functionalization was omitted evidencing that the surface chemistry is mandatory at this step (see SI figureS2).

The different steps corresponding to proteins adsorption on the quartz sensors were monitored in-situ by Quartz Crystal Microbalance with dissipation measurements. Typical sensorgrams obtained for gold and silicon AuNP-nanostructured sensors are depicted in Figure 3.

QCM-D curves in Figure 3 show that sequential injections of protein A, antibody and BSA result in significant negative shifts of the resonance frequency and concomitant increase of the dissipation evidencing their adsorption on the transducer surfaces.

Table 1 gathers frequency shifts measured upon stabilization for the AuNP-coated gold and silicon sensor chips. The data obtained for planar gold and planar silicon sensor chips in the same conditions, but by replacing for silicon the cysteamine molecule by APTES groups to generate amine function, are also shown in
Table 1 for comparison. The dissipation shifts and the standard deviations estimated on a minimum set of three experiments are shown with additional QCM data in the SI section (Table S2). The weak changes in dissipation allowed us to apply the Sauerbrey equation and determine the mass uptakes from which, considering the molecular weight of the different proteins used herein [56], we calculated the surface coverages for each surface (

Table 1).
The calculations reported in
Table 1 consider the entire mass change on the surface. However, one must keep in mind that water hydrodynamically trapped within the film is not taken into account and that it may increase the mass uptakes up to a factor of 4 (Höök et al., 2001). This may explain why the calculated antibody density is twice that of a complete monolayer (2.5 pmol/cm^2) [56] but does not impede the validity of relative comparison between QCM-D data obtained for protein adsorption on different surfaces.

By comparing the values obtained for the flat surfaces with those obtained from the nanostructured ones, the first observation is that whatever the substrates are, coverage in anti-SEA antibody is always the same. Indeed, on both silicon and gold sensors whether coated by AuNP or not, the coverage in anti-SEA is ca. 4 pmol/cm² with a standard deviation of 7.5 %. This result is in agreement with the low increase in the specific surface area induced by AuNP assembly on the surfaces. Indeed, if we consider an increase of $2\pi r^2$ per nanoparticle, and for an average density of approx. 20.10^9 particle/cm², the overall increase in the specific surface area would be ~ 5.7 %. When it comes to SEA capture, the input of AuNP structuration is clearly marked, in contrast with anti-SEA immobilization. The response of the $AuNP_{13}$-coated sensors upon SEA capture at a fixed concentration of 485 ng/mL was significantly higher compared to planar sensors, an increase of 32% and 56% was observed for gold and silicon surfaces, respectively. Considering that on all sensors surfaces, the anti-SEA coverage was identical, this improvement is certainly an evidence of a better accessibility of the recognition sites on the nanostructured sensors compared to the planar ones. The binding efficiencies, expressed as the SEA/anti-SEA ratio, were 1.3 and 1.4 for nanostructured gold and silicon sensors, respectively, and 0.8 to 1 for planar gold and silicon substrates (

Table 1). This observation corroborates the hypothesis of a better accessibility of the binding sites on the nanostructured substrates.

We assessed the possible influence of particle size and curvature by exploring the assembly of 40-nm diameter AuNP on gold substrates. Data gathered in

Table 1 show no significant difference in the amounts of Protein A, anti-SEA, and SEA adsorbed on the $AuNP_{13}$- compared to $AuNP_{40}$-coated gold sensors. Such a modification in particle diameter is therefore not sufficient to affect immunosensor construction and test.

Interestingly, the results obtained for gold and silicon flat surfaces are very similar showing a reproducibility of the measurements over time and an efficiency of the activation step whatever either the nature of the substrate or the surface chemistry applied using cysteamine or APTES for gold or silicon, respectively. The same observation can be made on nanostructured gold and silicon substrates for which identical responses are recorded upon SEA capture.

On the whole, although the amount of antibody binding sites was the same for all the sensor configurations, their accessibility was dramatically improved by AuNP nanostructuration. In what follows, we investigate the analytical performances of the nanostructured sensors.

3.4. *Analytical performances of nanostructured-SEA immunosensors*

$AuNP_{13}$-coated immunosensors were submitted to SEA solutions with variable concentration and dose-response curves were established by plotting -ΔF versus SEA concentration (Figure 4). Curve fitting of data was performed using the Langmuir isotherm equation

$\Delta F = \Delta F_{max}$ x [SEA]/([SEA] + K) where K refers to the dissociation constant for the direct detection format.

The calculated K and ΔF_{max} are summarized in Table 2.

The nanostructured piezoelectric immunosensors thus set up were able to detect and quantify SEA in the range between 50 and 500 ng/mL with an analysis time of 15-20 min (injection time + washing). Above a concentration of SEA of 500 ng/mL, the immunosensors' response was seen to reach saturation. The calculated saturation coverages given by the values of ΔF_{max} were quite similar, consistently with the identical values measured above for anti-SEA coverages on the different substrates. All the same, the constant K was significantly lower for the two AuNP-coated immunosensors. This indicates a higher apparent affinity for the nanostructured substrates and corroborates the hypothesis of a better accessibility of the antibody binding sites for the AuNP-modified QCM chips compared to the planar chips. The measured values, approx. 60 ng/mL which corresponds to 2.2 nM, are in the typical order of magnitude of an efficient antibody/antigen interaction.

To pursue the investigation of the possible effect of gold nanoparticles size, curve fitting for $AuNP_{13}$- and $AuNP_{40}$-coated gold surfaces were measured and compared (Table 2 and Figure S3, SI section). The two curves were again very similar and confirm that there is no significant contribution of particle size.
The limit of detection for the $AuNP_{13}$- nanostructured sensors calculated on the basis of a response ΔF = -1 Hz, is ca. 8 ng/mL (Table 2). This LOD is clearly improved in comparison with the data obtained on flat surfaces (20 ng/mL).

3.5.Sandwich amplification of nanostructured SEA immunosensors response

In our previous work, we had found out that, since piezoelectric sensors are mass sensors, the sensor response to the SEA analyte could be amplified by applying a revelation antibody after the antibody capture step (sandwich assay configuration) [55, 57]. The same polyclonal anti-SEA antibody was used in the sandwich assay format, as SEA has several epitopes, and the total frequency shift (SEA + washing + anti-SEA) was measured on the sensorgrams obtained for various concentrations of SEA. The corresponding calibration curve is depicted in Figure 5. To our delight, marked amplification of sensor response to analyte was observed and the LOD calculated for a theoretical ΔF of -1 Hz dropped down to ca. 1 ng/mL (Table 2), 7 times lower than the previously established LOD for the sandwich format on planar substrates.

4. Conclusion

Au and Si quartz crystal sensor chips were decorated with gold nanoparticles with the objectives of i) increasing their surface area, ii) modifying the surface topography to allow a better accessibility of the recognition sites. Prior to AuNP immobilization, similar surface chemistries were applied to functionalize silicon and gold substrates by attaching either aminosilane or aminethiol on the silicon or gold substrate surface, respectively to generate amine-terminated layers. Then, an acid-terminated thiol was reacted on the amine groups to form a mixed layer of thiol and amine offering multiple anchoring points for further attachment of gold nanoparticles. Spectroscopic characterizations of the functionalized layers showed differences in the reactivity of gold and silicon. Therefore, to achieve similar densities and dispersions on the planar substrates, gold nanoparticles were deposited

following different methods on the substrates: by immersion on gold and by flow on silicon. Sensing interfaces comprising anti-SEA antibody immobilized *via* affinity to protein A were built up on these nanostructured sensors and the resulting chips were used as piezoelectric transducers to capture and detect SEA in buffer medium. It appeared that, although the number of binding sites as determined from QCM measurements was the same for the planar and gold nanoparticle-coated sensors, the detection of SEA was significantly improved with the nanostructured sensors. This improvement is likely due to a better bioactivity of antibodies when bound to nanoparticles resulting from a better accessibility of the antigen binding sites. Amplification of sensor response was achieved by applying the polyclonal anti-SEA antibody after the analyte capture step which allowed decreasing the LOD down to 1 ng/mL.

Acknowledgement

This work was supported by the DIM Analytics programme funded by Region Ile de France, by the CNRS and by ANR-FWF joint project "NanoBioSensor", ANR-15-CE29-0026-02.

References

[1] Y. Le Loir, F. Baron, M. Gautier, Staphylococcus aureus and food poisoning, Genet Mol Res, 2(2003) 63-76.
[2] E.J. Schantz, W.G. Roessler, M.J. Woodburn, J.M. Lynch, H.M. Jacoby, S.J. Silverman, et al., Purification and some chemical and physical properties of staphylococcal enterotoxin A, Biochemistry, 11(1972) 360-6.
[3] M. Sharma, Lytic bacteriophages: Potential interventions against enteric bacterial pathogens on produce, Bacteriophage, 3(2013) e25518.
[4] P. Arora, A. Sindhu, N. Dilbaghi, A. Chaudhury, Biosensors as innovative tools for the detection of food borne pathogens, Biosens Bioelectron, 28(2011) 1-12.
[5] J. Homola, J. Dostálek, S. Chen, A. Rasooly, S. Jiang, S.S. Yee, Spectral surface plasmon resonance biosensor for detection of staphylococcal enterotoxin B in milk, Int J Food Microbiol, 75(2002) 61-9.
[6] W. Lian, D. Wu, D.V. Lim, S. Jin, Sensitive detection of multiplex toxins using antibody microarray, Anal Biochem, 401(2010) 271-9.
[7] M.B. Medina, A Biosensor method for a competitive immunoassay detection of staphylococcal enterotoxin B (SEB) in milk, J Rapid Methods Autom Microbiol, 13(2005) 37-55.
[8] M.B. Medina, A biosensor method for detection of staphylococcal enterotoxin A in raw whole egg, J Rapid Methods Autom Microbiol, 14(2006) 119-32.
[9] A.N. Naimushin, S.D. Soelberg, D.K. Nguyen, L. Dunlap, D. Bartholomew, J. Elkind, et al., Detection of Staphylococcus aureus enterotoxin B at femtomolar levels with a miniature integrated two-channel surface plasmon resonance (SPR) sensor, Biosens Bioelectron, 17(2002) 573-84.
[10] L. Rasooly, A. Rasooly, Real time biosensor analysis of Staphylococcal enterotoxin A in food, Int J Food Microbiol, 49(1999) 119-27.
[11] W.-C. Tsai, I.-C. Li, SPR-based immunosensor for determining staphylococcal enterotoxin A, Sens Actuators B Chem, 136(2009) 8-12.

[12] W.-C. Tsai, P.-J.R. Pai, Surface plasmon resonance-based immunosensor with oriented immobilized antibody fragments on a mixed self-assembled monolayer for the determination of staphylococcal enterotoxin B, Mikrochim Acta, 166(2009) 115-22.
[13] J.B. Delehanty, F.S. Ligler, A microarray immunoassay for simultaneous detection of proteins and bacteria, Anal Chem, 74(2002) 5681-7.
[14] M.E. Pekdemir, D. Erturkan, H. Kulah, I.H. Boyac, C. Ozgen, U. Tamer, Ultrasensitive and selective homogeneous sandwich immunoassay detection by Surface Enhanced Raman Scattering (SERS), Analyst, 137(2012) 4834-40.
[15] E. Temur, A. Zengin, I.H. Boyaci, F.C. Dudak, H. Torul, U. Tamer, Attomole sensitivity of staphylococcal enterotoxin B detection using an aptamer-modified surface-enhanced Raman scattering probe, Anal Chem, 84(2012) 10600-6.
[16] X. Yang, X. Zhao, X. Zuo, K. Wang, J. Wen, H. Zhang, Nucleic acids detection using cationic fluorescent polymer based on one-dimensional microfluidic beads array, Talanta, 77(2009) 1027-31.
[17] G.A. Campbell, M.B. Medina, R. Mutharasan, Detection of Staphylococcus enterotoxin B at picogram levels using piezoelectric-excited millimeter-sized cantilever sensors, Sens Actuators B Chem, 126(2007) 354-60.
[18] Z. Gao, F. Chao, Z. Chao, G. Li, Detection of staphylococcal enterotoxin C2 employing a piezoelectric crystal immunosensor, Sens Actuators B Chem, 66(2000) 193-6.
[19] J.L.N. Harteveld, M.S. Nieuwenhuizen, E.R.J. Wils, Detection of Staphylococcal Enterotoxin B employing a piezoelectric crystal immunosensor, Biosens Bioelectron, 12(1997) 661-7.
[20] N. Karaseva, T. Ermolaeva, A regenerable piezoelectric immunosensor on the basis of electropolymerized polypyrrole for highly selective detection of Staphylococcal Enterotoxin A in foodstuffs, Mikrochim Acta, 182(2015) 1329-35.
[21] M.G.R. Pimenta-Martins, R.F. Furtado, L.G.D. Heneine, R.S. Dias, M.d.F. Borges, C.R. Alves, Development of an amperometric immunosensor for detection of staphylococcal enterotoxin type A in cheese, J Microbiol Methods, 91(2012) 138-43.
[22] M.S. DeSilva, Y. Zhang, P.J. Hesketh, G.J. Maclay, S.M. Gendel, J.R. Stetter, Impedance based sensing of the specific binding reaction between Staphylococcus enterotoxin B and its antibody on an ultra-thin platinum film, Biosens Bioelectron, 10(1995) 675-82.
[23] S. Dong, G. Luo, J. Feng, Q. Li, H. Gao, Immunoassay of Staphylococcal Enterotoxin C1 by FTIR Spectroscopy and Electrochemical Gold Electrode, Electroanalysis, 13(2001) 30-3.
[24] W. Jin, K. Yamada, M. Ikami, N. Kaji, M. Tokeshi, Y. Atsumi, et al., Application of IgY to sandwich enzyme-linked immunosorbent assays, lateral flow devices, and immunopillar chips for detecting staphylococcal enterotoxins in milk and dairy products, J Microbiol Methods, 92(2013) 323-31.
[25] T. Kasama, M. Ikami, W. Jin, K. Yamada, N. Kaji, Y. Atsumi, et al., Rapid, highly sensitive, and simultaneous detection of staphylococcal enterotoxins in milk by using immuno-pillar devices, Anal Methods, 7(2015) 5092-5.
[26] P. Skládal, Piezoelectric biosensors, TrAC, Trends Anal Chem, 79(2016) 127-33.
[27] L. Reverté, B. Prieto-Simón, M. Campàs, New advances in electrochemical biosensors for the detection of toxins: Nanomaterials, magnetic beads and microfluidics systems. A review, Anal Chim Acta, 908(2016) 8-21.
[28] B. Stephen Inbaraj, B.H. Chen, Nanomaterial-based sensors for detection of foodborne bacterial pathogens and toxins as well as pork adulteration in meat products, J Food Drug Anal, 24(2016) 15-28.

[29] J. Breault-Turcot, J.F. Masson, Nanostructured substrates for portable and miniature SPR biosensors, Anal Bioanal Chem, 403(2012) 1477-84.
[30] Y. Li, H. Schluesener, S. Xu, Gold nanoparticle-based biosensors, Gold Bull, 43(2010) 29-41.
[31] X. Cao, Y. Ye, S. Liu, Gold nanoparticle-based signal amplification for biosensing, Anal Biochem, 417(2011) 1-16.
[32] A.-L. Morel, S. Boujday, C. Méthivier, J.-M. Krafft, C.-M. Pradier, Biosensors elaborated on gold nanoparticles, a PM-IRRAS characterisation of the IgG binding efficiency, Talanta, 85(2011) 35-42.
[33] A.-L. Morel, R.-M. Volmant, C. Méthivier, J.-M. Krafft, S. Boujday, C.-M. Pradier, Optimized immobilization of gold nanoparticles on planar surfaces through alkyldithiols and their use to build 3D biosensors, Colloids Surf B Biointerfaces, 81(2010) 304-12.
[34] P.-T. Chu, C.-S. Lin, W.-J. Chen, C.-F. Chen, H.-W. Wen, Detection of Gliadin in Foods Using a Quartz Crystal Microbalance Biosensor That Incorporates Gold Nanoparticles, J Agric Food Chem, 60(2012) 6483-92.
[35] R.A. Fonseca, J. Ramos-Jesus, L.T. Kubota, R.F. Dutra, A nanostructured piezoelectric immunosensor for detection of human cardiac troponin T, Sensors (Basel), 11(2011) 10785-97.
[36] A. Makaraviciute, T. Ruzgas, A. Ramanavicius, A. Ramanaviciene, A QCM-D Study of Reduced Antibody Fragments Immobilized on Planar Gold and Gold Nanoparticle Modified Sensor Surfaces, Key Eng Mater, 605(2014) 340-3.
[37] H. Chen, J.-H. Jiang, Y. Huang, T. Deng, J.-S. Li, G.-L. Shen, et al., An electrochemical impedance immunosensor with signal amplification based on Au-colloid labeled antibody complex, Sens Actuators B Chem, 117(2006) 211-8.
[38] D.-Q. Tang, D.-J. Zhang, D.-Y. Tang, H. Ai, Amplification of the antigen–antibody interaction from quartz crystal microbalance immunosensors via back-filling immobilization of nanogold on biorecognition surface, J Immunol Methods, 316(2006) 144-52.
[39] H. Wang, C. Lei, J. Li, Z. Wu, G. Shen, R. Yu, A piezoelectric immunoagglutination assay for Toxoplasma gondii antibodies using gold nanoparticles, Biosens Bioelectron, 19(2004) 701-9.
[40] H. Wang, J. Wu, J. Li, Y. Ding, G. Shen, R. Yu, Nanogold particle-enhanced oriented adsorption of antibody fragments for immunosensing platforms, Biosens Bioelectron, 20(2005) 2210-7.
[41] A. Papadopoulou-Bouraou, J. Barrero-Moreno, M. Lejeune, F. Brétagnol, M. Manso, A. Valsesia, et al., Plasma-Polymerized Allylamine-Based Label-Free Piezoelectric Immunosensor Platform: Characterization and Application, Sens Mat, 18(2006) 353–66.
[42] X. Jia, Q. Xie, Y. Zhang, S. Yao, Simultaneous Quartz Crystal Microbalance-Electrochemical Impedance Spectroscopy Study on the Adsorption of Anti-human Immunoglobulin G and Its Immunoreaction at Nanomaterial-modified Au Electrode Surfaces, Anal Sci, 23(2007) 689-96.
[43] X. Chu, Z.-L. Zhao, G.-L. Shen, R.-Q. Yu, Quartz crystal microbalance immunoassay with dendritic amplification using colloidal gold immunocomplex, Sens Actuators B Chem, 114(2006) 696-704.
[44] Y. Ding, Y.Y. Zhou, H. Chen, D.D. Geng, D.Y. Wu, J. Hong, et al., The performance of thiol-terminated PEG-paclitaxel-conjugated gold nanoparticles, Biomaterials, 34(2013) 10217-27.

[45] X. Jin, X. Jin, L. Chen, J. Jiang, G. Shen, R. Yu, Piezoelectric immunosensor with gold nanoparticles enhanced competitive immunoreaction technique for quantification of aflatoxin B1, Biosens Bioelectron, 24(2009) 2580-5.
[46] N.H. Kim, T.J. Baek, H.G. Park, G.H. Seong, Highly sensitive biomolecule detection on a quartz crystal microbalance using gold nanoparticles as signal amplification probes, Anal Sci, 23(2007) 177-81.
[47] S.B. Reddy, D.E. Mainwaring, M. Al Kobaisi, P. Zeephongsekul, J.V. Fecondo, Acoustic wave immunosensing of a meningococcal antigen using gold nanoparticle-enhanced mass sensitivity, Biosens Bioelectron, 31(2012) 382-7.
[48] J. Han, J. Zhang, Y. Xia, L. Jiang, Highly sensitive detection of the hepatotoxin microcystin-LR by surface modification and bio-nanotechnology, Colloids Surf A, 391(2011) 184-9.
[49] M. Ben Haddada, M. Hübner, S. Casale, D. Knopp, R. Niessner, M. Salmain, et al., Gold Nanoparticles Assembly on Silicon and Gold Surfaces: Mechanism, Stability and Efficiency in Diclofenac Biosensing, J Phys Chem C, (2016).
[50] M. Ben Haddada, J. Blanchard, S. Casale, J.-M. Krafft, A. Vallée, C. Méthivier, et al., Optimizing the immobilization of gold nanoparticles on functionalized silicon surfaces: amine- vs thiol-terminated silane, Gold Bull, 46(2013) 335-41.
[51] L. Dalstein, M. Ben Haddada, G. Barbillon, C. Humbert, A. Tadjeddine, S. Boujday, et al., Revealing the Interplay between Adsorbed Molecular Layers and Gold Nanoparticles by Linear and Nonlinear Optical Properties, J Phys Chem C, 119(2015) 17146-55.
[52] J.W. Slot, H.J. Geuze, A Method to Prepare Isodisperse Colloidal Gold Sols in the Size Range 3–17 nm, Ultramicroscopy, 15(1984) 383.
[53] S. Boujday, S. Nasri, M. Salmain, C.M. Pradier, Surface IR immunosensors for label-free detection of benzo a pyrene, Biosens Bioelectron, 26(2010) 1750-4.
[54] D. Mercier, S. Boujday, C. Annabi, R. Villanneau, C.-M. Pradier, A. Proust, Bifunctional Polyoxometalates for Planar Gold Surface Nanostructuration and Protein Immobilization, J Phys Chem C, 116(2012) 13217-24.
[55] M. Salmain, M. Ghasemi, S. Boujday, J. Spadavecchia, C. Técher, F. Val, et al., Piezoelectric immunosensor for direct and rapid detection of staphylococcal enterotoxin A (SEA) at the ng level, Biosens Bioelectron, 29(2011) 140-4.
[56] S. Boujday, A. Bantegnie, E. Briand, P.-G. Marnet, M. Salmain, C.-M. Pradier, In-Depth Investigation of Protein Adsorption on Gold Surfaces: Correlating the Structure and Density to the Efficiency of the Sensing Layer, J Phys Chem B, 112(2008) 6708-15.
[57] M. Salmain, M. Ghasemi, S. Boujday, C.-M. Pradier, Elaboration of a reusable immunosensor for the detection of staphylococcal enterotoxin A (SEA) in milk with a quartz crystal microbalance, Sens Actuators B Chem, 173(2012) 148-56.

Authors Biography

Maroua Ben Haddada received her a PhD at University Pierre & Marie Curie under the supervision of S. Boujday and M. Salmain. Her research focuses on the engineering of biofunctionalized gold nanoparticles and their further use for surface functionalization and biosensing of pollutants and toxins.

Michele Salmain graduated from the Ecole Nationale Superieure de Chimie de Paris in 1987 and completed a PhD at the Université Pierre & Marie Curie in 1990, in the interface discipline coined Bioorganometallic chemistry. As researcher appointed by the CNRS, she develops research projects dealing with the organometallic chemistry of proteins and the development of immunosensors.

Souhir Boujday received Ph.D degree in 2002 on the interfacial molecular recognition between transition metal complexes and silica surface. She joined the University Pierre & Marie Curie as Associate Professor in 2004 and defended her habilitation to research supervision in 2012. She spent 2 years 2014-2016 as Visiting Professor at Nanyang Technological University, Singapore. Her research work is focused on surface chemistry and biosensors development including the use of metallic nanoparticles for an enhanced sensitivity.

Figure 1. A: XPS (N1s Photopeak) and B: PM-IRRAS data obtained upon CEA adsorption on gold and further grafting of activated MUA.

Figure 1

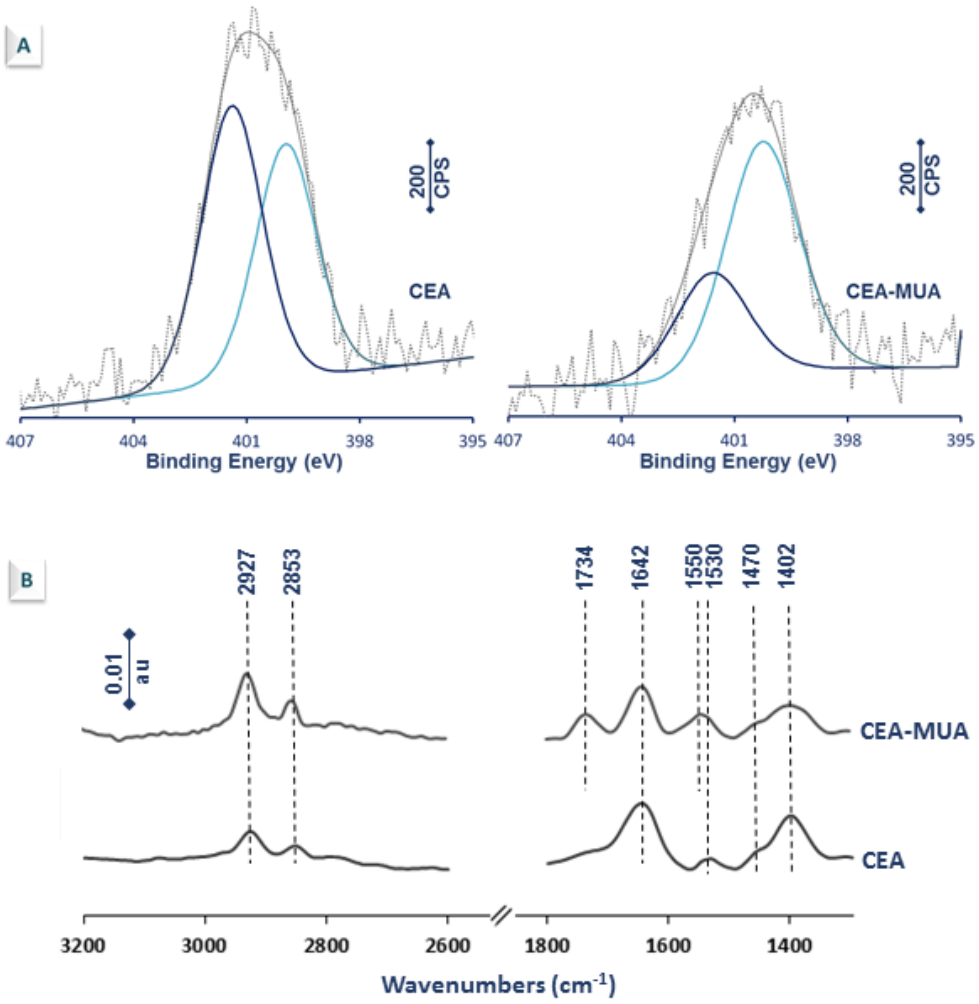

Figure 2. Frequency and dissipation shifts measured during immobilization of $AuNP_{13}$ on thiol-functionalized (a) Au and (c) Si QCM sensor; (b and d) SEM image of QCM Au and Si sensor modified with $AuNP_{13}$ respectively.

Figure 2

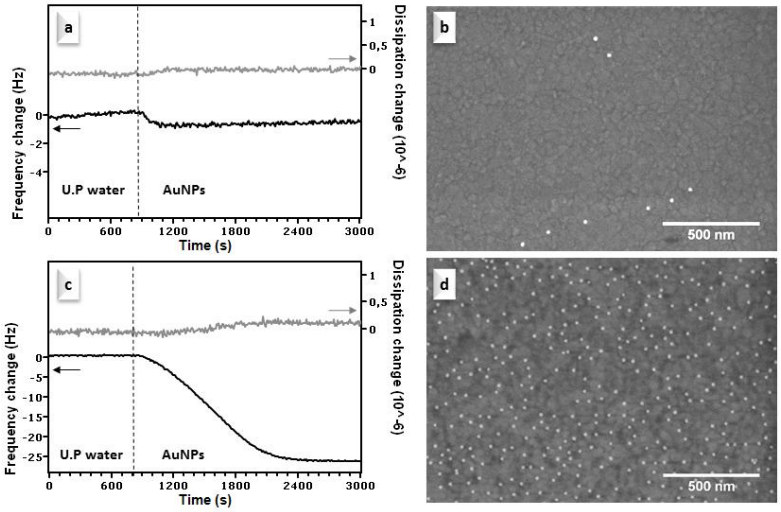

Figure 3. Sensorgrams recorded during sensing layer build up and response to SEA at 485 ng/mL in PBS-BSA on (a) $AuNP_{13}$-Au and (b) $AuNP_{13}$-Si quartz crystal sensors.

Figure 3

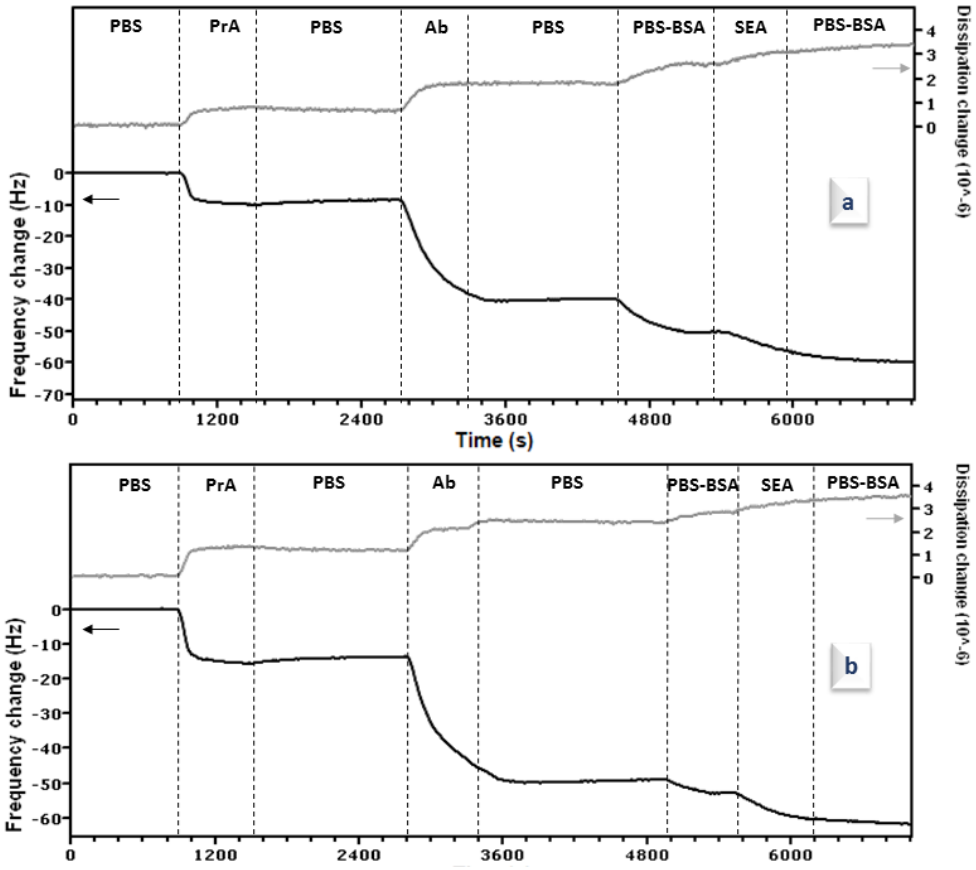

Figure 4. Detection of SEA at different concentrations in the direct format using $AuNP_{13}$ coated (a) Au and (c) Si sensors and mathematical curve fitting according to the Langmuir equation (b and d respectively).

Figure 4

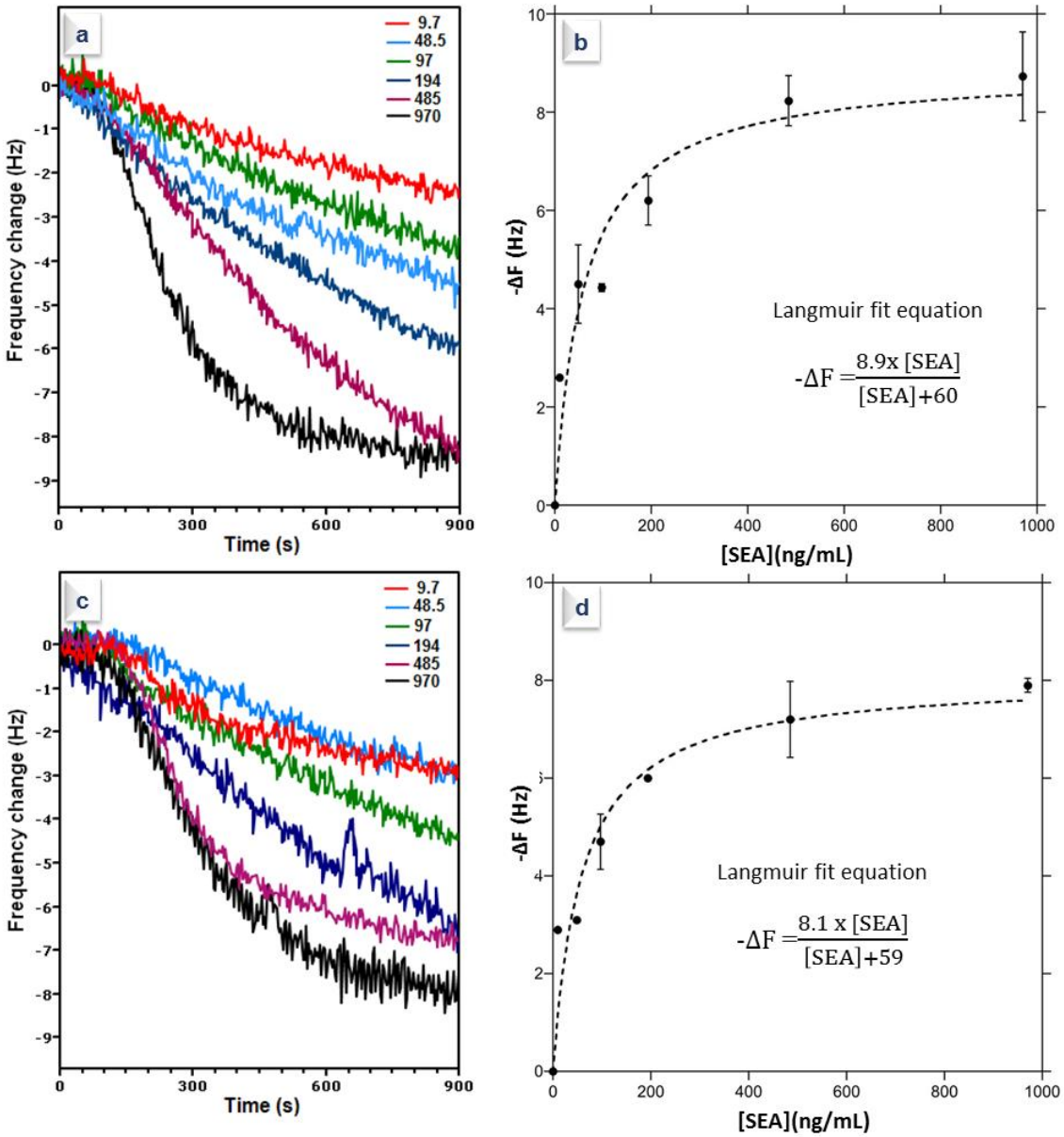

Figure 5. (a) Response of AuNP$_{13}$-coated Si QCM sensors after injection of SEA at different concentrations followed by the injection of antibody anti-SEA (10 mg/L) in PBS–BSA. (b) Calibration curves for SEA in the direct (●) ($-\Delta F = 8 \times [SEA]/([SEA] + 35)$, R = 0.96) and

sandwich (□) formats (-ΔF = 49 × [SEA]/([SEA] + 51), R = 0.982). The dotted lines result from mathematical curve fitting according to the Langmuir equation

Figure 5

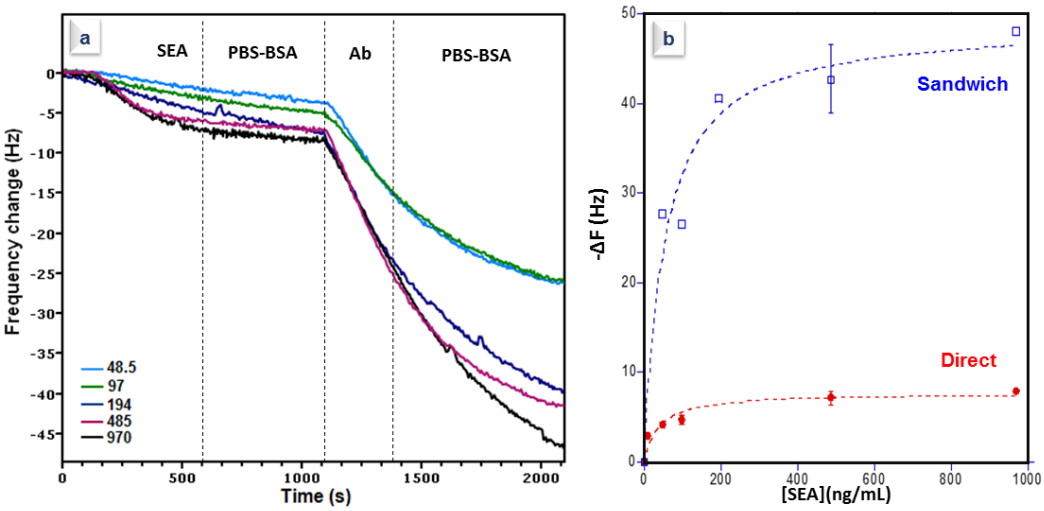

Scheme 1. Immobilization of gold nanoparticles on Au (A) and Si (B) quartz crystal sensors and post-functionalization of immobilized AuNP (C)

Scheme 1

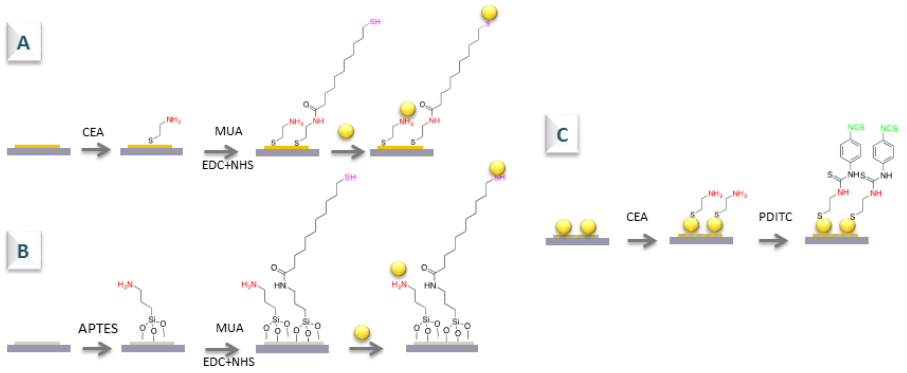

Table 1. Frequency shifts, surface coverages and Ag/Ab ratio measured for nanostructured (*$AuNP_{13}$-coated and $AuNP_{40}$-coated)* and planar QCM sensor chips upon flowing Protein A

(20 mg/L), anti-SEA (10 mg/L) and SEA (485 ng/mL).

Step	Sensor	*$AuNP_{13}$-coated Au*	*$AuNP_{40}$-coated Au*	*Planar Au*[a]	*$AuNP_{13}$-coated Si*	*Planar Si*
PrA	ΔF (Hz)	-7.0	-7.9	-6.9	-9.4	-7.0
	Γ (pmol/cm^2)	2.7	3.1	2.7	3.7	2.7
Anti-SEA	ΔF (Hz)	-33.9	-34.8	-33.0	-32.6	-33.7
	Γ (pmol/cm^2)	4.0	4.1	3.9	3.8	4.0
SEA	ΔF (Hz)	-8.2	-7.9	-6.2	-8.3	-5.3
	Γ (pmol/cm^2)	5.2	5.0	3.9	5.2	3.4
SEA/Anti-SEA		1.3	1.2	1.0	1.4	0.8

[a] ref. [55]

Table 2. Calibration curve parameters for direct and sandwich format assays on AuNP-coated and bare Au and Si quartz sensors

Immunosensor configuration	ΔF_{max} (Hz)	K (ng/mL)	R	LOD (ng/mL)[a]
Direct format				
$AuNP_{13}$-Au	8.1 ± 0.8	60 ± 22	0.966	7.6 ± 1.8
$AuNP_{40}$-Au	9.0 ± 0.8	91 ± 25	0.989	11.4 ± 3.1
Planar Au[b]	9.8 ± 0.6	183 ± 37	0.990	20.8 ± 4.2
$AuNP_{13}$-Si	8.1 ± 0.8	59 ± 23	0.960	8.3 ± 3.7
Sandwich format				
$AuNP_{13}$-Si, sandwich	49 ± 4	51 ± 16	0.982	1.1 ± 0.4
Planar Au[b,c]	23	151	0.987	7

[a] calculated for ΔF = -1 Hz; [b] ref. [55], the sandwich antibody used in this measurement was different